Journal of Additive Manufacturing Technologies
DOI: 10.18416/JAMTECH.2111589

Infinite Science | Publishing

A numerical approach to assess the impact of the SLM laser parameters on thermal variables

M. Majeed[1*], H. M. Khan[2], G. Wheatley[1], and R. Situ[1]

[1] College of Science and Engineering, Townsville, Australia.
[2] Fatih Sultan Mehmet Vakif University, ALUTEAM, Sutluce Mahallesi, Beyoglu, Istanbul, Turkey.
[*] Corresponding author, email: mobeen414@gmail.com
First two authors have equal contributions

Abstract

Due to extraordinarily high heating and cooling rates, understanding the selective laser melting (SLM) process remains a challenge. To evaluate the impact of processing parameters on distinct underlying surfaces, a three-dimensional finite element model is presented. To forecast the temperature distribution inside a finite solid model, a moving Gaussian heat source was created to scan the model with temperature-dependent material properties. In the finite model, the impact of processing factors such as laser power, scan rate, and scan spacing were investigated to measure thermal variables such as cooling rate, thermal gradient, and solidification rate in a layer with solid and powder bases. The maximum track temperature was observed to be increasing over the whole track length, which had a substantial influence on the thermal gradient, cooling rate, and solidification rate. The maximum track temperature, melt pool form, and thermal variables were shown to be strongly influenced by laser power and scan speed when compared to scan spacing. Furthermore, the underlying base had a substantial influence on the observed temperature values and melt pool shape.

Keywords: Selective laser melting, Finite element analysis, 316L, Cooling rate, Temperature gradient, Additive manufacturing, Powder bed.

1. Introduction

Additive manufacturing (AM) has progressed from a prototype method to full-fledged commercial part production for a variety of sectors, including biomedical, aerospace, defense, automotive, and heavy machinery [1]. It has grown in prominence in recent decades as a result of its design flexibility, simplicity of production, reduced material waste, and capacity to construct complicated structures. AM is a technology that allows for the simple creation of complex structures such as lattice materials in a single step with unique mechanical properties that would otherwise be almost difficult to create using any available conventional techniques [1-3]. Selective Laser Melting (SLM) is a powder-based AM technique used to produce near net form metal components with few intermediary stages and assembly. To build 3D structures, the method needs selective scanning of small powder particles layer by layer [4, 5]. Strictly speaking, laser powder interaction determines the whole process and, as such, must be thoroughly researched in order to optimize the manufacturing technique for components with optimal strength and achievable microstructural characteristics.

Despite the many benefits of the SLM process, there are still many obstacles to overcome to make SLM parts commercially acceptable. Dimensional inaccuracies, porosity, absence of fusion, and powder agglomeration to the surface are some of the primary difficulties with this technique. These flaws significantly reduce the mechanical performance of additive components [1]. However, by adjusting process settings and post-processing conditions, these problems may be greatly reduced. The laser scanning of a powder bed induces complicated chemical and physical processes within a melt-pool, influencing various thermal variables such as temperature gradient and cooling speeds. These factors are crucial for assessing the final microstructure of additive components, which in turn play a significant role in creating the final mechanical characteristics of the components [6, 7]. However, the SLM process is so fast that assessing thermal factors experimentally is almost difficult [8]. As a result, the designers were forced to seek an alternate technique in numerical modeling in order to gain a thorough understanding of the process.

Several attempts have been made to simulate the thermo-physical system in the SLM process [4, 8-10]. Numerical models based on heat conduction, for example, may be used to assess the 3D transient temperature distribution, measuring thermal variables, microstructural evolutions, and thermal stresses [11-14]. Luo et al. created a 3-D nonlinear transient thermomechanical linked FEM to monitor temperature and stress field during SLM in a multilayer model [15]. Foroozmeher et. al. successfully estimated the

temperature and melt pool size of 316 L material during the multitrack study of the SLM process [16]. Rosso et al. predicted melt pool size and the absence of fusion flaws, which agreed well with their experimental results [17]. Criales et. al. has predicted 2 D temperature profile and melt pool geometry of Inconel 625 metal powder[18]. They have evaluated the effect of energy and material density on the thermal characteristics. Chen et. al performed the finite element analysis, to calculate the melting-solidification path during SLM of ceramic [19]. Majeed et. al. has evaluated the behavior of thermal variables with passing laser [8]. Waqar et. al. performed multitrack and multilayer analysis to investigate the thermal behavior and melt pool characteristics [20].

Thermo-mechanical modeling of the SLM process provides a quick, dependable, and cost-effective method for analyzing laser scanning behavior across the powder bed [21]. This allows the designer to make significant modifications to the final structure and improve processing conditions during the laser scanning of complicated regions. Therefore, a 3D transient multi-track and multi-layer thermal model was constructed in this work to explore the heat transport on two distinct underlying surfaces. To measure temperature fields, thermal variables, and assess melt pool shape change with laser position, the model solves the equations of conservation of mass, momentum, and energy. The temperature-dependent mechanical and physical characteristics of the powder bed, support structure, and solid substrate are all included in the model. Four distinct laser parameter sets were used to thoroughly examine the influence of laser power, scan rate, and scan spacing on thermal variables in different tracks and layers of a thermal model.

2. Methodology

This work makes use of 316L stainless steel, which is a common additive material for the SLM method and has several uses in aerospace, automotive, and medicinal fields, making it an important material for scientific research [22, 23]. The effect of process factors such as laser power, scan speed, hatching, and energy density is explored in the FEM model, which is shown in Table 1. Laser process parameters have a significant impact on the final part characteristics of components, which need thorough evaluation, especially in structures with intricate features.

Table 2 shows the different sets of laser processing parameters utilized in this study. The selection of four different parameter sets was to include the effect of laser power, scanning speed, and scan spacing on the thermal variables and the formed melt pools of the selected FE model. This process uses a Gaussian heat source symmetric around the central axis with reducing intensity and maximum at the center. It can be described using following equation [8].

Table 1. Laser processing parameters utilized in this study.

Process parameters	Numerical value
Laser Power	200 W, 250 W
Scan speed	700 mm/s, 1000 mm/s
Hatch spacing	70 μm, 110μm
Laser spot size	100 μm
Track length	800 μm
Penetration depth	100 μm

Table 2. Different combination of laser processing parameters utilized in this study.

Model No.	Laser power (W)	Scan speed (mm/s)	Scan spacing (μm)
1	200	700	110
2	200	1000	110
3	250	1000	110
4	250	1000	70

$$q = \frac{2\mathcal{E}P}{\pi R^2 S} exp\left(\frac{2\left((x-{x_0}^2+(y-y_0-Vt)^2\right)}{R^2}\right) exp\left(-\frac{|z-z_0|}{S}\right) \quad (1)$$

Here, x, y and z are Cartesian coordinates in space. V is scanning speed, R is spot radius set at 100 μm, Ɛ is material absorptivity = 0.4. S = 100 μm is penetration depth of laser in 316L stainless steel.

During laser scanning, a part of impinged heat is absorbed by material powder, a part is lost through convection and radiation. But the total heat is conserved as expressed by the following equation [8].

$$k\frac{\partial T}{\partial \eta} - q_v + h_c(T - T_0) + \sigma\varepsilon(T^4 - {T_0}^4) \quad (2)$$

Where, T is temperature, t is time of temperature attained, k is thermal conductivity of 316 L, q_v is heat generated by laser, hc is Stefan Boltzmann constant, σ convective heat coefficient, and ε is emissivity of material. T_0 = 303K is room temperature. After impingement of laser, the material faces continuous melting and solidification. The latent heat for this process can be given as

Considering the melting and solidification phenomenon within SLM process, the latent heat for phase change is expressed in the form of enthalpy, H, as a function of temperature [8]

$$H = \int \rho c dT \quad (3)$$

Where, ρ is the material density and c are the specific heat capacity. The thermal conductivity of the loose powder is given as;

$$k_p = k_s(1 - \emptyset) \quad (4)$$

Where, $\emptyset$ is the porosity of the powder bed and it is defined as;

$$\emptyset = \frac{\rho_s - \rho_p}{\rho_s} \quad (5)$$

Where, ρ_s and ρ_p are the densities of solid and powder, respectively with $\rho_p = 0.4\,\rho_s$. The temperature dependent specific heat, isotropic thermal conductivity, and density of 316 L powder and solid are shown in Fig 1.

2.1 Finite element model

A cubical model of size 0.5 X 1 X 0.35 mm with plane symmetry about the Y-Z plane is used in this investigation, as illustrated in Fig 2. The meshing's element size is 5 µm. The model base was utilized to depict the substrate or previously solidified region underneath the scanning zone. Along the track length, the model base was divided into two halves. The first half had the solid base, while the second half was assigned the powder base. The entire model has two layers with a thickness of 40 µm. Both strata have two tracks with hatch spacings of 110 µm and 70 µm for different scenarios.

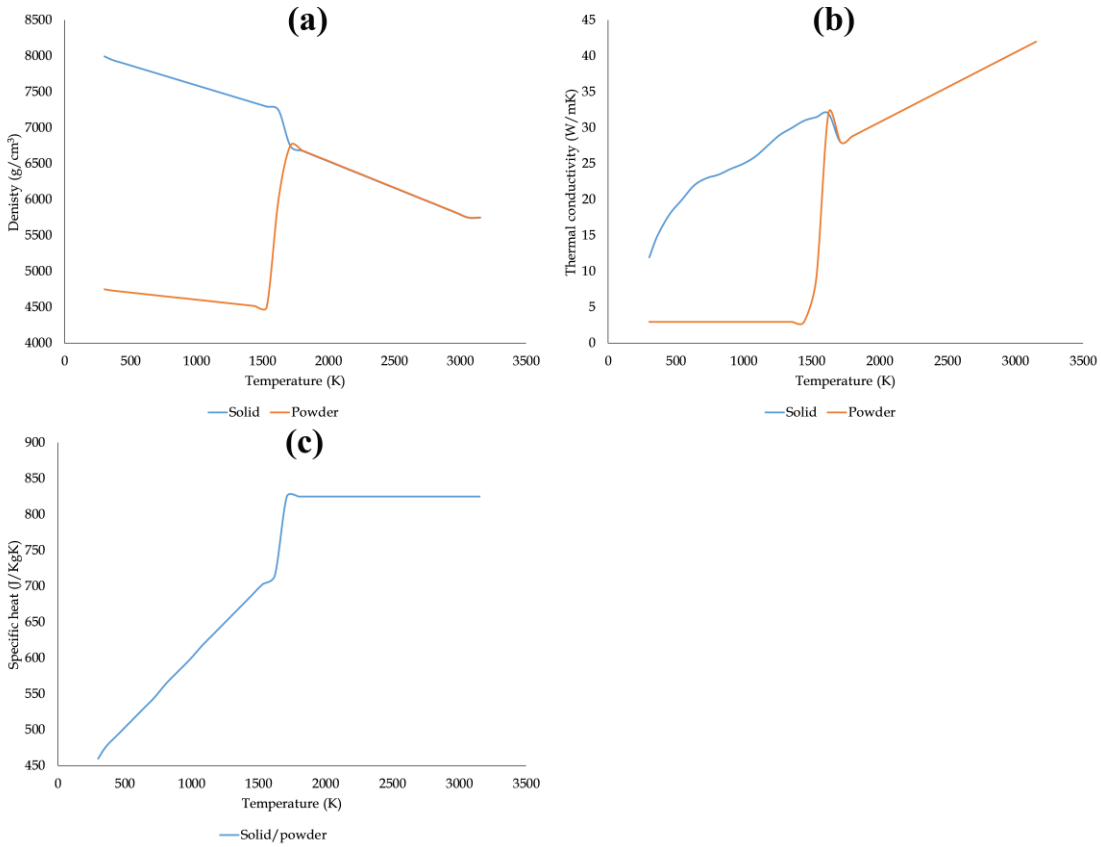

Fig 1. Temperature dependent (a) density, (b) thermal conductivity, and (c) specific heat of 316L stainless steel.

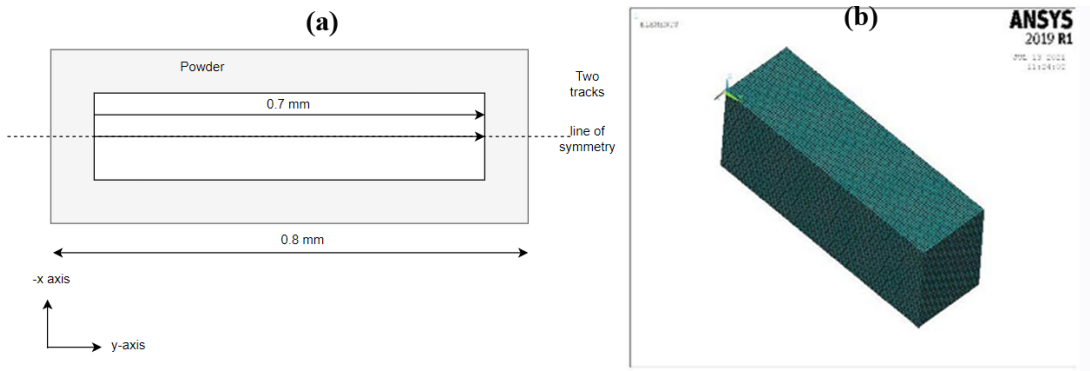

Fig 2. (a) Finite element model and (b) schematic plan view of the scanning region.

3. Results and discussion

3.1 Maximum track temperature

Laser parameters play a key role in the determination of maximum temperature inside a melt pool and the melt pool shape and size. The energy incident into the powder bed can be measured according to the following equation.

$$\varphi = \frac{P}{vhl} \quad (6)$$

Where, the energy density φ is dependent on laser power P, scanning speed v, scan spacing h, and layer thickness l. There are other important factors like the diameter of a laser beam, powder packing density, underlying base type to the scanning layer, and powder material properties that can also influence the amount of energy density entering into the powder bed. In the present study, four factors were given major consideration, such as laser power, scan speed, scan spacing, and the underlying base material to the scanning layer.

The process of laser scanning introduces huge amount of energy into the scanning layer that quickly dissipates through the surrounding powder particles and the substrate [5]. The substrate can also include the previously solidified layers in case the laser scanning is away from the substrate. Since powder particles are loosely bounded with each other, heat dissipation through them is far low than the solid structure. As a result, the heat transfer from the scanned laser is far higher through the substrate or the previously solidified layer. Therefore, it is highly recommended to have an interconnected solid region around the scanned laser for fast heat dissipation. This is the reason why small scan spacing and layer thickness in the SLM process can play a key role in avoiding heat retention in the scanned layer. However, while producing complex structures, such as overhang structures, cooling channels, or specially designed lattice materials, the regions surrounding the scanning area may not be solid. As a result, the SLM process becomes more challenging and difficult to comprehend. This study is primarily focusing on three factors, such as maximum melt pool temperature, thermal variables (cooling rate, thermal gradient, and solidification rate), and melt-pool size, as a result of changing laser processing parameters (laser power, scan speed, scan spacing) and underlying base material (solid base or powder base).

As observed from Fig 3, the maximum melt pool temperature at the beginning of laser scanning is very small compared to the middle or end part of the track. This is because of no prior thermal history of the powder particles. As the laser moves forward, the heat retention keeps on increasing inside newly formed melt-pools until a pseudo steady state (PSS) is reached. The PSS is defined when the increase in temperature of a track nearly stops, as shown by the dotted point in Fig 3(a). The PSS is dependent on several factors that includes laser processing parameters and the underlying base material. In other words, the amount of energy density is a prime factor in identifying the PSS state. The more the energy density, longer is the time to achieve the PSS state or higher is the PSS temperature. The PSS is an important element in a thermal model representing a moving Gaussian heat source to identify the track length of the model, since choosing a large track length is expected to not produce any significant change in studies on maximum track temperature or thermal variables than the small track length, which passed the PSS state. In the present study, the model 1 with higher incident energy density at 200 W laser power, 700 mm/s scanning speed, and 110 µm scan spacing resulted in maximum melt pool temperature of about 2853 K.

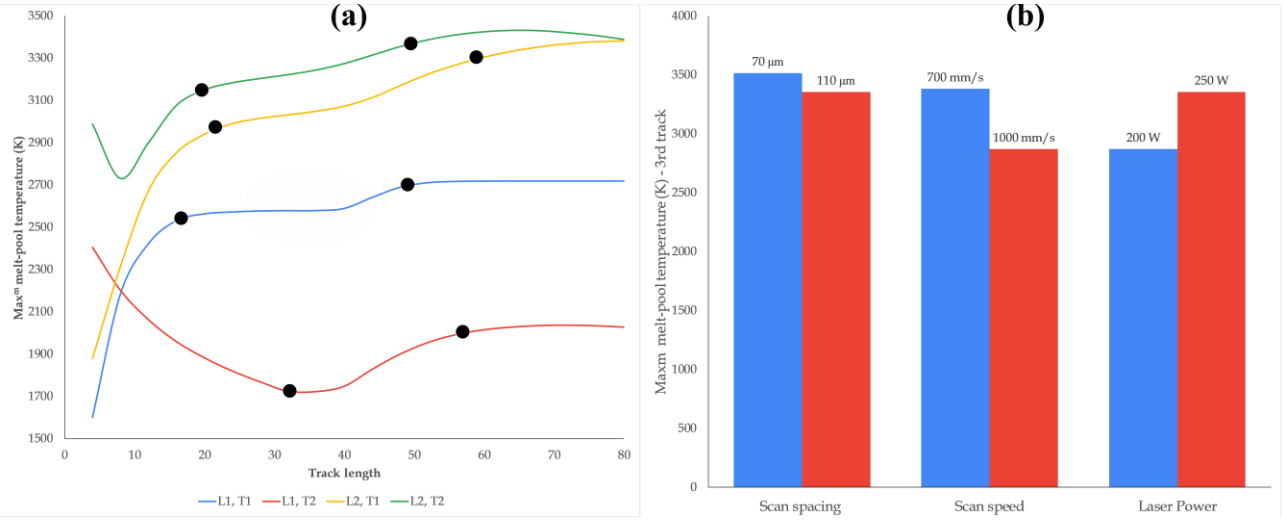

Fig 3. (a) change in maximum melt pool temperature along the total track length and (b) melt pool temperature variation with respect to the changing laser processing parameters.

Between the laser process parameters, the increase in laser scanning speed and scan spacing produced a lower maximum track temperature and a relatively early PSS, while the laser power had an opposite effect.

Compared to the laser power and scan speed, the effect of scan spacing on maximum track temperature or PSS state was nearly negligible even though the change in scan spacing was quite significant. Because the influence of scan spacing can only be seen on the second track in each layer, and the scan spacing values used are already low, the net change in maximum temperature was smaller than what was seen with other parameters. As the laser moves forward and enters the region with the powder base, a small jump in maximum melt pool temperature was observed. This small jump was because of the 316L powder material compared to the solid base. By contrast, the PSS time was observed relatively quicker in regions with the powder base. This was because the melt pool was already at high temperature and the laser entry into the powder base produced only a slight fluctuation in temperature.

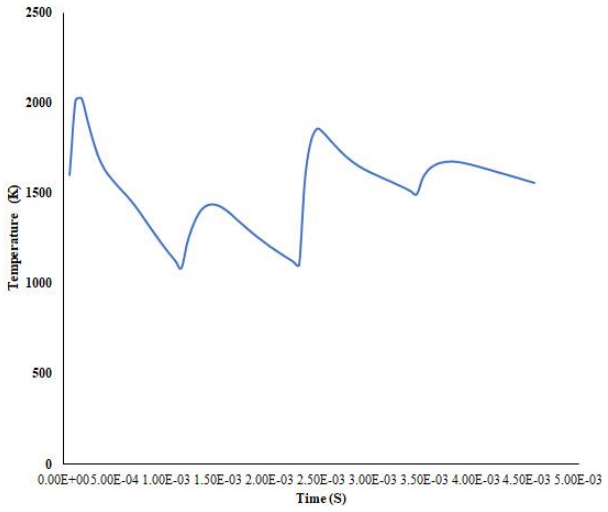

Fig 4. Temperature time graph of a nodal point in the first track of model 1 above the solid base.

The influence of track or layer addition on maximum track temperature and PSS state was also made in this study. Although the trend followed by the maximum track temperature or PSS state was nearly similar on all the tracks, their values were found increasing with the track addition. This is again attributed to some heat retention by the previous track that contributes temperature increment in the second track. Fig 4 shows the temp-time graph of a nodal point in the middle of the first track above the solid base. The graph clearly exhibits incomplete dissipation of the heat after the passing of the laser. Heat retention in the second layer was greater during the scanning of the second track than in the first layer due to inadequate heat dispersion. As a result of the underlying previously scanned tracks of the first layer, the temperature reduction of the second track of the second layer was comparatively smaller.

When the laser started scanning the region above the powder base in the first track, the heat retention was greater than in the center of the solid base. As a result, the temperature at the start of the second track was extremely high, and it only began to drop and homogenize as the laser continued to proceed down the track length. Later, when the laser enters the powder base, the maximum track temperature or PSS trend became similar to the first track. Compared to the track addition, the effect of layer addition on maximum temperature or PSS time was more significant, as observed from Fig 3.

3.2 Melt pool size

The incident of laser on the powder bed quickly melts the powder particles, resulting in a melt pool that follows the Gaussian map of the heat source, such that the oval shape returns after the laser scanning. The melt-pool resembles like a fish tail when observed from the built side, which grows in size, as the laser moves forward. The underlying base material, whether solid or powder base, and laser processing parameters can alter the melt pool dynamics resulting in their varied sizes and shape. In return, the size and shape of the grain structure inside the melt pool as well as the crystallographic orientation also changes depending on the amount of incident energy density. In the present study, the melt pool was found varying with laser processing parameters and the underlying base material type.

At the beginning of the scanning process, due to the absence of nodal thermal history and the underlying solid base, the heat retention was poor, causing a relatively smaller melt-pool size than the one observed later with the powder base. Since powder particles are poor in heat dissipation, they retain heat for longer time. This results in deeper and wider melt pool shapes compared to the region above the solid base. The maximum melt pool temperature directly relates to the melt-pool shape and size, and therefore, the melt-pool size, such as its length, width, and depth, follows the similar trend, as observed with the maximum track temperature. The more the energy density, higher was the maximum temperature, bigger was the melt pool size. Hence, increase in laser power or decrease in scanning speed or scan spacing produces a larger melt pool shape, as observed in Fig 5b. Compared to the laser power and scanning speed, the effect of scan spacing on melt pool size was relatively smaller.

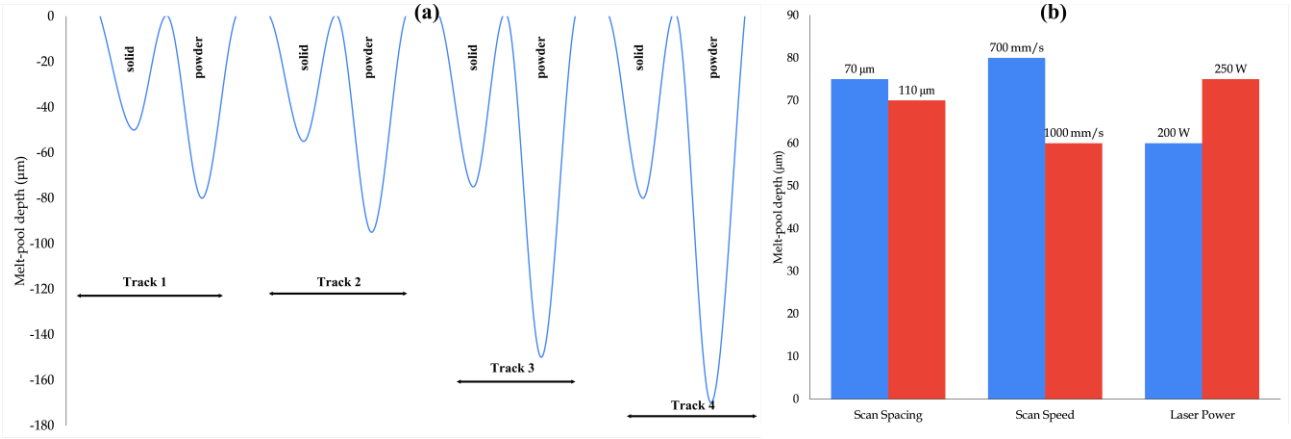

Fig 5. change in melt pool depth along the total track length and (b) melt pool depth variation with respect to the changing laser processing parameters.

The effect of track and layer addition also followed the same trend, as seen in the maximum track temperature case. The track or layer addition resulted in a relatively higher temperature reach in the scanned tracks, causing melting of extra powder particles, hence larger melt-pools, as shown in Fig 5a. Having a large melt-pool over the previously solidified layers is relatively good since it can eliminate the pores formed during the first scanning. However, deeper melt-pools over the powder base like the overhang regions or cooling channels can drastically affect the shape and size of the geometry [4]. Therefore, it is extremely important to control the laser processing parameters depending on the geometrical position. One way is to increase the supporting materials in regions above the powder base or to apply low energy density in the down-skin regions prior to full scanning with the standard parameters [2, 5]. The latter case can ensure small melt pool depth, resulting in fewer dross formation, hence retaining the geometrical accuracy of the predesign CAD model.

Fig 6 shows the variation in melt pool length and width with respect to the chosen processing parameters. Similar to the melt-pool depth, the variation in melt pool length and width was wider when high laser power and low scan speed or scan spacing were utilized.

3.3 Thermal variables

From the temperature field, the temperature gradient (G) and cooling rate (Cr) can be determined directly, whereas the solidification rate (R) is measured from the combination of G and Cr (G/Cr). The cooling rate is proportional to the size of the grain features in the fusion zone, while the solidification rate is used to identify the shape of solidification structures such as planar, cellular, columnar, dendritic, and equiaxed dendritic (from a high G/R value to a low one).

Fig 7a shows the effect of energy input on temperature gradient along Y axis (TGY). As the laser traverse along the track length, the amount of incident energy density increases, and since the powder particles are poor in dissipating the heat generated during the laser scanning, the heat retention in the melt pools along the track increases. As a result, the temperature gradient values reduces. Compared to the scanning region above

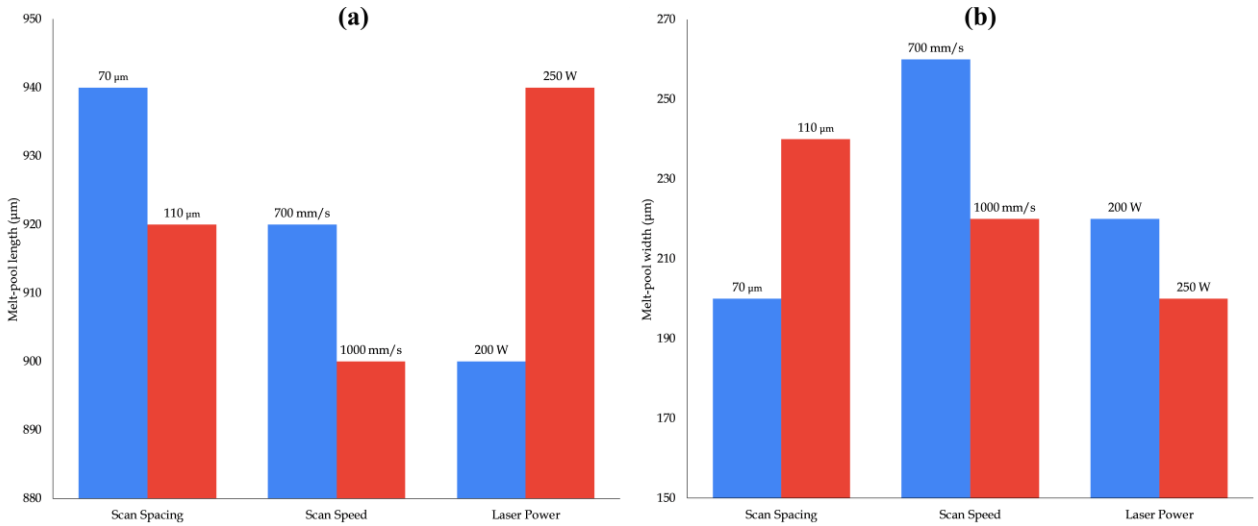

Fig 6. (a) melt pool length variation and (b) melt pool width variation with respect to the changing laser processing parameters.

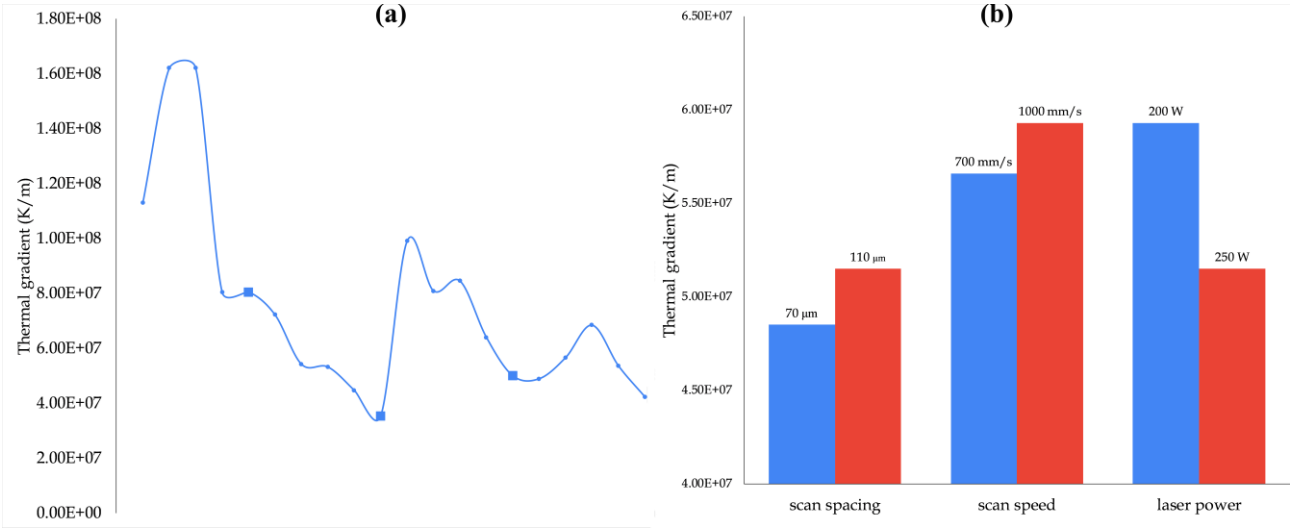

Fig 7. (a) change in thermal gradient values along the total track length and (b) thermal gradient variation with respect to the changing laser processing parameters. Square box represents the end of a track.

the solid base, the scanning point above the powder base showed a significant drop in the temperature gradient due to the heat accumulation in the melt pool. With the addition of new track and layer, the maximum track temperature was already found increasing in Fig 3, their effect on the temperature gradient also showed the similar behavior.

In the second track of the first layer, the high temperature at the track initiation was shown due to the nearby powder zone. Furthermore, due to the high heat transfer from the first track, the temperature gradient also showed the similar behavior. The high heat accumulation resulted in lower thermal gradient values at the track initiation, which was found decreasing along the track over the solid base. Not shown here but the temperature gradient behavior was similar to the maximum track temperature on the second track of the second layer where the temperature gradient values were found decreasing for a short while before increasing again as the laser moves ahead. The change in temperature gradient in the second layer was relatively negligible due to the underlying previously solidified metal base. In Fig 7a, the square dots represent the end of a track.

Between the laser scanning parameters, the effect of laser power, scan speed, and scan spacing on thermal gradient was identical to the one observed with the maximum track temperature, as shown in Fig 7b. High laser power, low scan speed, and small scan spacing were all found to reduce the temperature gradient values in all the four tracks of the present thermal model. The effect on the thermal gradient due to scan spacing was relatively lower than the other two laser parameters. It is understood that the heat induced by the incident laser beam on a single track is by far mainly proportional to the laser power and scan speed. By the

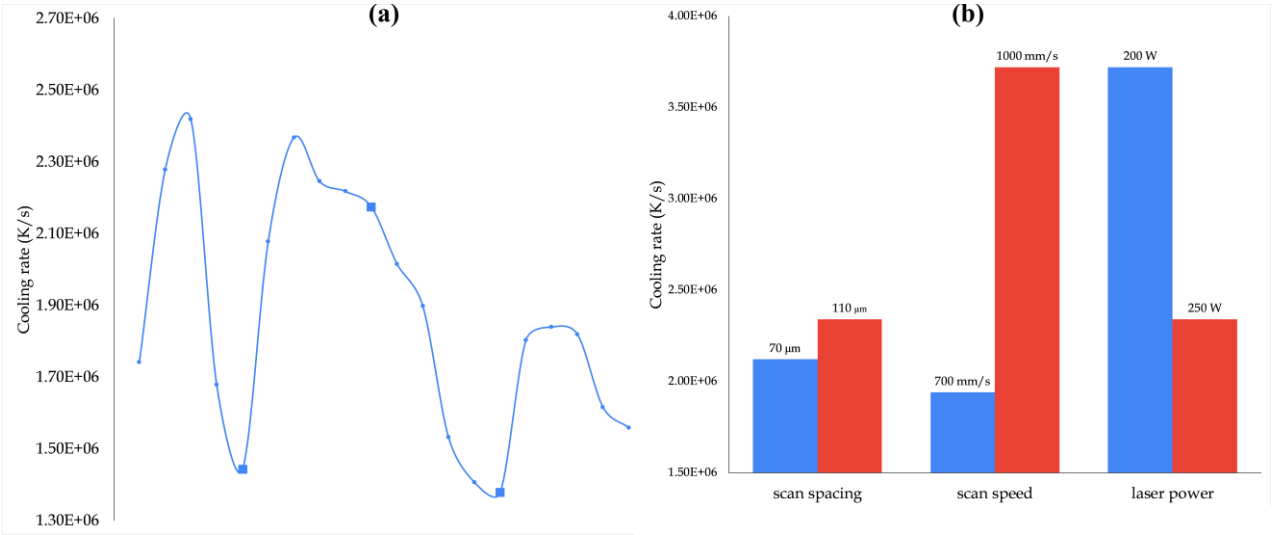

Fig 8. (a) change in cooling rate values along the total track length and (b) cooling rate variation with respect to the changing laser processing parameters.

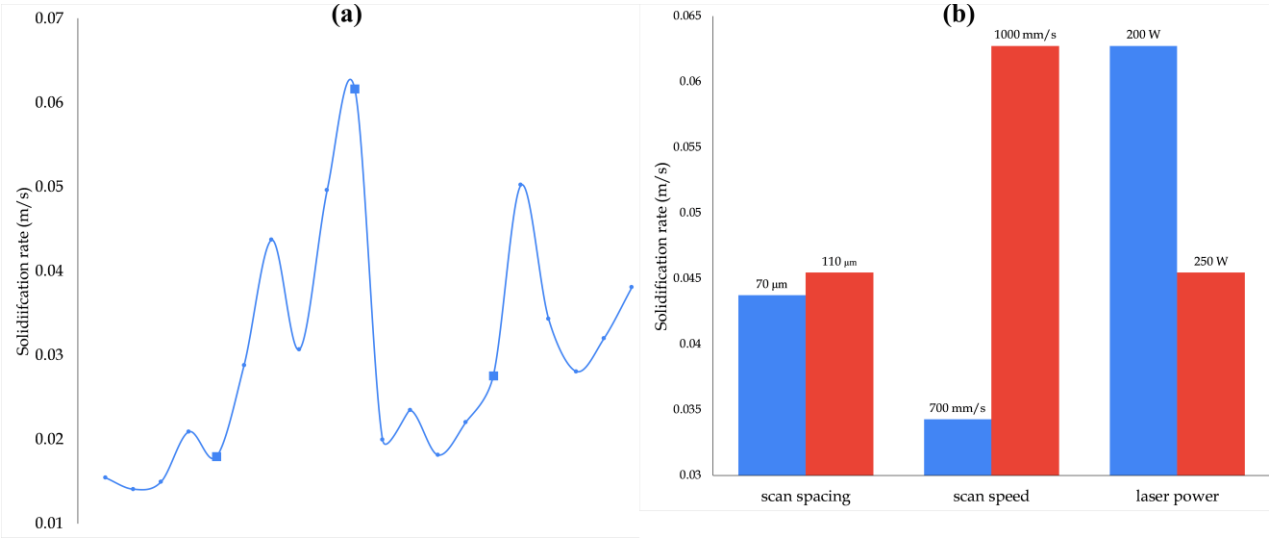

Fig 9. (a) change in solidification rate values along the total track length and (b) solidification rate variation with respect to the changing laser processing parameters.

time the laser scans the adjacent region, the heat transfer from the adjacent track is relatively limited compared to the energy induced by the laser power and scan speed. Therefore, the change in maximum melt pool temperature and other thermal variables due to scan spacing was relatively far lower than the one observed with the other two examined laser parameters.

The cooling rate in the SLM process is far too high compare to any existing conventional method, and it has a direct effect on the grain shape formed within the melt pool. The high cooling rate in the SLM process is attributable to the melt pool structure's high degree of heat dispersion. The higher the heat dissipation, the faster the cooling rate, and the finer the grain structure, which is why grain structures generated in the SLM melt pool are finer than those achieved by traditional methods[24]. Fig 8a depicts the change in cooling rate over the whole track length, which is comprised of four tracks, with square dots indicating the end of each track. In this study, the cooling rate was measured between the maximum melt pool temperature until the time when the material begins to solidify. As the laser begins to scan the track, the cooling rate increases until it reaches a PSS condition. Later, the cooling rate slows owing to heat accumulation in the succeeding melt pools along the track length, and this tendency continues in the powder area. Due to the significant heat retention, the scanning track over the powder base had lower cooling rate values when compared to the solid base. In the subsequent tracks, the cooling rate behavior was similar to the case observed in the temperature gradient, where the cooling rate was found decreasing with the addition of new tracks or layers, primarily due to high heat retention in the melt pools compared to the one observed in the first track. The tracks in the second layer indicate a somewhat smaller drop in cooling rate than the tracks in the first layer due to the solidified region underneath it. Furthermore, the decrease in cooling rate was largely attributable to heat retention in tracks. The cooling rate was shown to decrease with rising laser power and decreasing scanning speed or scan spacing among the laser processing parameters, as observed from Fig 8b. This was attributed to the amount of energy density induced by the scanning laser beam, which was higher at high laser power and low scanning speed and scan spacing.

As shown in Fig 9, the solidification rate is related to the energy input, cooling rate, and temperature gradient. The rate of solidification was observed to increase with the addition of a track and layer. At 200 W laser power, 700 mm/s scan speed, and 110 µm scan spacing, the solidification rate rises from 15.4 mm/s in the first track to 36.85 mm/s in the fourth track. With the addition of a new track, the cooling rate increases and the thermal gradient decreases, resulting in a minor rise in solidification rate and fast movement of the solidification front. Furthermore, when compared to different energy inputs, the solidification rate was shown to decrease with incident energy density, implying that when laser power increased or scan speed or scan spacing decreased, the solidification rate decreased (Fig 9b).

4. Conclusions

Understanding the selective laser melting (SLM) process remains difficult because of extremely fast heating and cooling rates. A three-dimensional finite element model is developed to analyze the influence of laser processing parameters on different underlying surfaces. A moving Gaussian heat source was constructed to scan the model using temperature-dependent material characteristics in order to anticipate the temperature distribution inside a finite solid model. The influence of processing parameters such as laser power, scan rate, and scan spacing on thermal variables such as cooling rate, thermal gradient, and solidification rate in a layer with solid and powder bases was examined in the finite model. The maximum track temperature was found increasing over the whole track length, having a significant impact on the thermal gradient, cooling rate,

and solidification rate. When compared to scan spacing, laser power and scan speed were shown to have a substantial impact on maximum track temperature, melt pool shape, and thermal variables. In addition, the underlying base (solid or powder) had a significant impact on the measured temperature values and melt pool shape, such that the powder base showed poor heat dissipation, thereby reducing thermal variables and increasing the maximum melt pool temperature and melt pool size.

Conflict of interest: Authors state no conflict of interest.

References

1. Khan, H.M., et al., Influence of the post-processing operations on surface integrity of metal components produced by laser powder bed fusion additive manufacturing: a review. Machining Science and Technology, 2020. **25**(1): p. 118-176.
2. Oter, Z.C., et al., Support optimization for overhanging parts in direct metal laser sintering. Optik, 2019. **181**: p. 575-581.
3. Khan, H.M., et al., Improving the surface quality and mechanical properties of selective laser sintered PA2200 components by the vibratory surface finishing process. SN Applied Sciences, 2021. **3**(3): p. 364.
4. Khan, H.M., et al., Numerical investigation of heat current study across different platforms in SLM processed multi-layer AlSi10Mg. Optik, 2018. **170**: p. 82-89.
5. Khan, H.M., M.H. Dirikolu, and E. Koç, Parameters optimization for horizontally built circular profiles: Numerical and experimental investigation. Optik, 2018. **174**: p. 521-529.
6. DebRoy, T., et al., Additive manufacturing of metallic components–process, structure and properties. Progress in Materials Science, 2018. **92**: p. 112-224.
7. Kruth, J.-P., M.-C. Leu, and T. Nakagawa, Progress in additive manufacturing and rapid prototyping. Cirp Annals, 1998. **47**(2): p. 525-540.
8. Majeed, M., H. Khan, and I. Rasheed, Finite element analysis of melt pool thermal characteristics with passing laser in SLM process. Optik, 2019. **194**: p. 163068.
9. Peyre, P., et al., Experimental and numerical analysis of the selective laser sintering (SLS) of PA12 and PEKK semi-crystalline polymers. Journal of Materials Processing Technology, 2015. **225**: p. 326-336.
10. Foteinopoulos, P., A. Papacharalampopoulos, and P. Stavropoulos, On thermal modeling of Additive Manufacturing processes. CIRP Journal of Manufacturing Science and Technology, 2018. **20**: p. 66-83.
11. Michaleris, P., Modeling metal deposition in heat transfer analyses of additive manufacturing processes. Finite Elements in Analysis and Design, 2014. **86**: p. 51-60.
12. Patil, R.B. and V. Yadava, Finite element analysis of temperature distribution in single metallic powder layer during metal laser sintering. International Journal of Machine Tools and Manufacture, 2007. **47**(7): p. 1069-1080.
13. Loh, L.-E., et al., Numerical investigation and an effective modelling on the Selective Laser Melting (SLM) process with aluminium alloy 6061. International Journal of Heat and Mass Transfer, 2015. **80**: p. 288-300.
14. Gouge, M., et al., Experimental validation of thermo-mechanical part-scale modeling for laser powder bed fusion processes. Additive Manufacturing, 2019. **29**: p. 100771.
15. Luo, C., et al., Finite element analysis of temperature and stress fields during the selective laser melting process of thermoelectric SnTe. Journal of Materials Processing Technology, 2018. **261**: p. 74-85.
16. Foroozmehr, A., et al., Finite Element Simulation of Selective Laser Melting process considering Optical Penetration Depth of laser in powder bed. Materials & Design, 2016. **89**: p. 255-263.
17. Bruna-Rosso, C., A.G. Demir, and B. Previtali, Selective laser melting finite element modeling: Validation with high-speed imaging and lack of fusion defects prediction. Materials & Design, 2018. **156**: p. 143-153.
18. Criales, L.E., Y.M. Arısoy, and T. Özel, Sensitivity analysis of material and process parameters in finite element modeling of selective laser melting of Inconel 625. The International Journal of Advanced Manufacturing Technology, 2016. **86**(9): p. 2653-2666.
19. Chen, X., et al., Microstructure and mechanical properties of the austenitic stainless steel 316L fabricated by gas metal arc additive manufacturing. Materials Science and Engineering: A, 2017. **703**: p. 567-577.
20. Waqar, S., et al., Numerical investigation of thermal behavior and melt pool morphology in multi-track multi-layer selective laser melting of the 316L steel. The International Journal of Advanced Manufacturing Technology, 2021. **112**(3): p. 879-895.
21. Majeed, M., et al., Finite element analysis of thermal behavior in maraging steel during SLM process. Optik, 2020. **208**: p. 164128.
22. Yasa, E., et al., Charpy impact testing of metallic selective laser melting parts. Virtual and Physical Prototyping, 2010. **5**(2): p. 89-98.
23. Khairallah, S.A., et al., Laser powder-bed fusion additive manufacturing: Physics of complex melt flow and formation mechanisms of pores, spatter, and denudation zones. Acta Materialia, 2016. **108**: p. 36-45.
24. Thijs, L., et al., Strong morphological and crystallographic texture and resulting yield strength anisotropy in selective laser melted tantalum. Acta Materialia, 2013. **61**(12): p. 4657-4668.